Acta Crystallographica Section F
Structural Biology and Crystallization Communications
ISSN 1744-3091

Crystallization and preliminary X-ray crystallographic characterization of a public CMV-specific TCR in complex with its cognate antigen

Jean-Baptiste Reiser,[a] François Legoux,[b,c] Paul Machillot,[a] Emilie Debeaupuis,[b,c] Béatrice Le Moullac-Vaydie,[b,c] Anne Chouquet,[a] Xavier Saulquin,[b,c] Marc Bonneville[b,c]* and Dominique Housset[a]*

[a]Institut de Biologie Structurale Jean-Pierre Ebel, UMR 5075 (CEA, CNRS, UJF, PSB), 41 Rue Jules Horowitz, F-38027 Grenoble, France, [b]INSERM, UMR 892, Institut de Recherche Thérapeutique de l'Université de Nantes, 8 Quai Moncousu, BP 70721 F-44007 Nantes, France, and [c]Université de Nantes, Nantes, France

Correspondence e-mail: bonnevil@nantes.inserm.fr, dominique.housset@ibs.fr

Received 27 July 2009
Accepted 18 September 2009

The T-cell response to human cytomegalovirus is characterized by a dramatic reduction of clonal diversity in patients undergoing chronic inflammation or immunodepression. In order to check whether all the selected high-avidity T-cell clones recognize the immunodominant pp65 peptide antigen $pp65_{495–503}$ (NLVPMVATV) presented by the major histocompatibility complex (MHC) molecule HLA-A2 in a similar manner, several public high-affinity T-cell receptors (TCRs) specific for the $pp65_{495–503}$–HLA-A2 complex have been investigated. Expression, purification and crystallization were performed and preliminary crystallographic data were collected to 4.7 Å resolution for the RA15 TCR in complex with the $pp65_{495–503}$–HLA-A2 complex. Comparison of the RA15–$pp65_{495–503}$–HLA-A2 complex molecular-replacement solution with the structure of another high-affinity $pp65_{495–503}$–HLA-A2-specific TCR, RA14, shows a shared docking mode, indicating that the clonal focusing could be accompanied by the selection of a most favoured peptide-readout mode. However, the position of the RA15 Vβ domain is significantly shifted, suggesting a different interatomic interaction network.

1. Introduction

Human cytomegalovirus (HCMV) is a ubiquitous β-herpesvirus that infects 60–90% of the population. HCMV persists in a latent stage after the primary infection and can undergo transient reactivations. Although HCMV infections are kept in check by the immune system of healthy individuals, they can cause life-threatening diseases in immunodeficient patients (Sissons *et al.*, 2002). Cytotoxic T cells (CTLs) play a central role in controlling HCMV reactivation (Borysiewicz *et al.*, 1988; Quinnan *et al.*, 1984; McLaughlin-Taylor *et al.*, 1994; Wills *et al.*, 1996; Saulquin *et al.*, 2000) and the predominant CTL response is directed against the viral tegument protein pp65 (Wills *et al.*, 1996; Engstrand *et al.*, 2000). In individuals sharing the widespread HLA-A*0201 allele (referred to as A2), HCMV-specific CTLs recognize the same epitope $pp65_{495–503}$ (NLVPMVATV), hereafter referred to as NLV (Wills *et al.*, 1996; Diamond *et al.*, 1997; Peggs *et al.*, 2002). During chronic inflammation (*e.g.* in rheumatoid arthritis patients) and immunodepression, a dramatic reduction in clonal diversity occurs, resulting in the selection of a few dominant clones bearing high-affinity TCRs (Trautmann *et al.*, 2005). We have recently determined the crystal structures of the immunodominant NLV peptide bound to A2 in isolation or in complex with a high-avidity public TCR expressed by a predominant CTL clone (RA14) derived from a rheumatoid arthritis (RA) patient (Trautmann *et al.*, 2005) and have gained insight into the mechanisms underlying clonal focusing upon chronic antigen stimulation (Gras, Saulquin *et al.*, 2009). Here, we present preliminary X-ray diffraction data for another high-avidity NLV–A2 specific TCR, RA15, in complex with NLV–A2. This TCR shares the same Vα domain (TRAV24–TRAJ49, according to IMGT nomenclature; Lefranc, 2001) with RA14 but has a different Vβ domain (TRBV6-1 instead of TRBV6-5) and lacks some of the

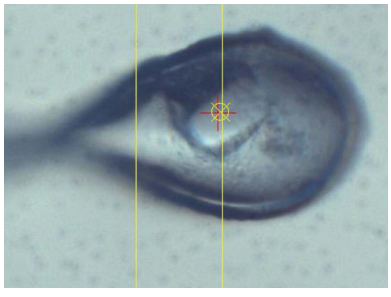

essential NLV-contacting residues identified in RA14. The structure of RA15 in complex with NLV–A2 would therefore be extremely useful to check whether the extraordinary clonal focusing that occurs upon chronic reactivation is accompanied by the selection of a common NLV–A2 readout mode. The molecular-replacement solution indicates at least a convergent mode of docking.

2. Experimental methods

2.1. RA15 TCR cloning

Total RNA was isolated with TRIzol (Invitrogen) from 5×10^6 RA15 T-cell clones. cDNAs encoding the V and C ectodomain of the α-chain and β-chain were obtained by RT-PCR using the following primers: 5′-CCATATGAATGCTGGTGTCACTCAGACCCC-3′ and 5′-GGAATTCTTAATCACAACCACCACCACGATCTTGGTCTGCTCTACCCCAGGCCTCGGCGCTGAC-3′ for the β-chain and 5′-CCATATGATACTGAACGTGGAACAAGGTCC-3′ and 5′-ACTCGAGTTTACAACCACCACCATCGTTTTCTGGGCTGGGGAAGAAGGTGTCTTCTGG-3′ for the α-chain. The PCR products were cloned into the pET-22b vector (Novagen). The resulting constructs were checked by sequencing.

However, attempts to obtain soluble RA15 TCR using this construct inexorably led to aggregates of TCR and an unsuitable yield of soluble protein for protein crystallization. In 2003, Boutler and coworkers demonstrated the efficacy of introducing non-native interchain disulfide bonds between the two constant domains in order to produce soluble TCRs without altering either the pMHC-binding capacity or the ternary complex crystallization (Boulter *et al.*, 2003). Cysteine codons were then introduced into pET22b-RA15α and pET22b-RA15β by PCR mutagenesis. Complementary primers were designed in order to mutate into cysteines (bold codons) Thr48 in TRAC (5′-GATGTGTATATCACAGACAAA**TGT**GTGCTAGACATGAGGTCTATG-3′ and 5′-CATAGACCTCATGTCTAGCAC-**ACA**TTTGTCTGTGATATACACATC-3) and Ser57 in TRBC (5′-GGTGCACAGTGGGGTC**TGT**ACAGACCCGCAGCCC-3′ and 5′-GGGCTGCGGGTCTGT**ACA**GACCCCACTGTGCACC-3′). These primers were then used with the QuikChange II kit (Stratagene, La Jolla, California, USA) and the pET22b constructs previously obtained as PCR templates. The site-directed mutagenesis results were confirmed by DNA sequencing.

2.2. Protein expression and purification of RA15 TCR

Cysteine-mutated RA15 α-chain and β-chain were produced separately as inclusion bodies in *Escherichia coli* strain BL21 (DE3) RIPL (Stratagene, La Jolla, California, USA) by the induction of a 3 l culture with 1 m*M* IPTG when the optical density reached 0.6 at a wavelength of 600 nm followed by 3 h incubation at 310 K. Inclusion bodies were isolated by cell lysis performed with a French press followed by successive washing and centrifugation steps with 15 ml of a solution containing 50 m*M* Tris pH 8, 100 m*M* NaCl, 0.5% Triton X-100, 1 m*M* DTT. The last wash step was made with a solution containing the same constituents apart from Triton X-100. Finally, inclusion bodies were solubilized in 8 *M* urea, 50 m*M* MES pH 6.5, 0.1 m*M* DTT and 0.1 m*M* EDTA and stored at 193 K before use.

Prior to refolding, 30 mg of both chains were mixed in 6 *M* guanidine–HCl, 50 m*M* MES pH 6.5, 10 m*M* EDTA, 2 m*M* DTT and 1 m*M* sodium acetate. RA15 TCR was then refolded by flash dilution into 500 ml of a cold (277 K) solution containing 3 *M* urea, 200 m*M* arginine–HCl, 150 m*M* Tris pH 8, 1.5 m*M* reduced glutathione and 0.15 m*M* oxidized glutathione. After incubation for 72 h at 277 K, the folding solution was dialyzed against 10 m*M* Tris pH 8.5 and 50 m*M* NaCl for 24 h and against 10 m*M* Tris pH 8.5 for 48 h at 277 K. The resulting protein solution was then concentrated using a 10 kDa membrane (Vivacell, Vivascience AG, Germany) and purified on a size-exclusion column (HiLoad 16/60 Superdex 200) equilibrated in 10 m*M* Tris pH 8.5 and 20 m*M* NaCl and connected to an FPLC system (Purifier 10, GE Healthcare Bio-Sciences AB, Uppsala, Sweden). The fractions containing soluble TCR were analyzed by Coomassie-stained SDS–PAGE electrophoresis under reducing and non-reducing conditions. Fractions containing equal quantities of both α-chain and β-chain were pooled, concentrated on Amicon with a cutoff of 30 kDa to a concentration of about 2 mg ml^{-1} and frozen at 193 K before further use. An aliquot was analyzed by mass spectrometry (MALDI–TOF) and confirmed the presence of RA15 TCR α/β dimers.

Prior to crystallization, samples of TCR were thawed and cleaned from aggregates and remaining single chains on an size-exclusion column (HiLoad 16/60 Superdex 75) equilibrated as previously and finally concentrated to a final concentration of 2–3 mg ml^{-1}.

Table 1
Crystallographic data-collection and refinement statistics.

Values in parentheses are for the highest resolution shell.

Data-collection statistics	
Space group	$P4_22_12$
Unit-cell parameters (Å)	$a = b = 99.14$, $c = 229.06$
Resolution (Å)	50.0–4.7 (4.95–4.7)
$R_{\rm merge}$† (%)	8.3 (40.7)
Completeness (%)	91.0 (92.7)
$I/\sigma(I)$	10.4 (2.99)
No. of reflections	21804 (3122)
No. of unique reflections	5856 (817)
Molecular-replacement statistics	
Resolution (Å)	15.0–4.7
Two-body rigid-body refinement	
Correlation coefficient (%)	68.2
R factor‡ (%)	52.3
Seven-body rigid-body refinement	
Correlation coefficient (%)	69.8
R factor‡ (%)	50.9

† $R_{\rm merge} = \sum_{hkl}\sum_i |I_i(hkl) - \langle I(hkl)\rangle|/\sum_{hkl}\sum_i I_i(hkl)$. ‡ $R = \sum_{hkl} \big||F_{\rm obs}| - |F_{\rm calc}|\big|/\sum_{hkl}|F_{\rm obs}|$. The *R* factor is calculated on all reflections.

2.3. Protein expression and purification of NLV-HLA-A2

HLA-A*0201 heavy chain and β_2-microglobulin were produced separately as described previously (Garboczi *et al.*, 1992; Bodinier *et al.*, 2000; Gras, Saulquin *et al.*, 2009). In brief, the A245V mutant of the HLA-A*0201 heavy chain tagged at the C-terminus with a biotinylation sequence was cloned into pHN1 expression vector as described in Bodinier *et al.* (2000). Recombinant proteins were produced as inclusion bodies in *E. coli* strain XA90F′LaqQ1. The inclusion bodies were resuspended in 8 *M* urea, 50 m*M* MES pH 6.5, 0.1 m*M* DTT, 0.1 m*M* EDTA, incubated overnight at 277 K and centrifuged for 30 min at 100 000*g*. The supernatant was collected and frozen at 193 K. The pMHC complex refolding step was performed by flash dilution of a mixture of 21 mg HLA-A*0201, 10 mg β_2-microglobulin and 10 mg of the NLV synthetic peptide into 350 ml 100 m*M* Tris pH 8.0, 400 m*M* L-arginine–HCl, 2 m*M* EDTA, 5 m*M* reduced glutathione, 0.5 m*M* oxidized glutathione with two Complete EDTA-free Cocktail protease-inhibitor tablets (Roche Diagnostics). The refolding solution was then incubated for 4–5 d at 277 K and concentrated with a 30 kDa cutoff membrane (Vivacell system). The pMHC complex was purified on a MonoQ 5/50 column with an FPLC system equilibrated in 10 m*M* Tris pH 8.0 buffer. It was eluted with

100–150 m*M* NaCl and concentrated with Amicon-10 or Amicon-30 devices to a final protein concentration of 2.5–3.5 mg ml^{-1}.

2.4. Crystallization

Prior to crystallization, RA15 TCR and HLA-A2–NLV were mixed in an equal molar ratio and at a final complex concentration of 3 mg ml^{-1}. Crystallization conditions were initially screened at 293 and 277 K using a Cartesian nanodrop crystallization robot available at the PSB HTX laboratory (Grenoble, France) and using JBScreen Classic screens (Jena Biosciences, Jena, Germany) and home-made screens with PEG (3350, 4000 and 6000), buffers at several pH values ($NaCH_3COO$, MES, HEPES and Tris) and salts (LiCl, $LiSO_4$, $CaCl_2$, $MgCl_2$ and $MgSO_4$).

Initial tiny crystals of the RA15–NLV–A2 complex were obtained after several weeks from these screens at 277 K and in conditions containing PEG 4000, Tris pH 8.0–8.5 and $MgSO_4$. These conditions were then refined using the hanging-drop technique by mixing 2 µl protein solution and 2 µl reservoir solution. The conditions were optimized by varying the concentration of PEG 4000 and $MgSO_4$ and the pH in the range 8.0–8.5 for the 100 m*M* Tris buffer.

The best crystals were obtained after several weeks at 277 K in conditions containing 17–18% PEG 4000, 100 m*M* Tris pH 8.5, 100–35 m*M* $MgSO_4$.

2.5. Diffraction data collection, processing and molecular replacement solution

Prior to being flash-frozen in liquid nitrogen for diffraction experiments, crystals were soaked in a cryoprotectant solution (mother liquor with the PEG 6000 concentration increased to 30%). Several crystals were tested for diffraction on beamline ID23-eh2 of the European Synchrotron Radiation Facility (ESRF, Grenoble, France) using an ADSC Q4 CCD detector at a wavelength of 0.873 Å. For most of the crystals, very weak diffraction was observed to 6 Å resolution. Only one crystal gave reasonable diffraction to 4.7 Å resolution (Fig. 1). A full data set was then collected at 100 K within 90° total angular range and a 1° oscillation step per image.

Data processing was performed using *XDS* (Kabsch, 1993) and is summarized in Table 1. The RA15–NLV–A2 complex crystals belonged to the tetragonal space group $P4_22_12$, with unit-cell parameters $a = b = 99.14$, $c = 229.06$ Å.

Structure determination of RA15–NLV–A2 was performed by molecular replacement with *AMoRe* (Navaza, 1994) using the RA14 and NVL–A2 crystal structures (Gras, Saulquin *et al.*, 2009; PDB code 3gsn) as initial and independent models. Clear contrasted rotation-function solutions were found for both the TCR and the pMHC independently and the translation function provided a unique solution for one TCR–pMHC ternary complex per asymmetric unit. Extra rigid-body refinement cycles were performed with *AMoRe* by defining seven rigid bodies (NLV MHCα1α2 and MHCα3 domains, β_2-microglobulin, TCR Vα, Cα, Vβ and Cβ domains) with a final *R* factor of 50.9% at 4.7 Å resolution (Table 1).

3. Results and discussion

We have previously solved the structure of the public RA14 TCR in complex with its cognate NLV–A2 epitope (Gras, Saulquin *et al.*, 2009). This structure highlighted the structural characteristics that explain the immunodominance of this particular TCR in response to NLV–A2 associated with HCMV reactivation. Particularly, the emergence of an optimal public solution from an oligoclonal antigen-specific repertoire after repeated HCMV stimulations seems to be based on a TCR with a very favourable combination of TRAV, TRAJ and TRBV translating into an optimal structural complementarity between the TCR and the pMHC surface. Moreover, a significant number of RA14 TCR-contacting amino acids appear to be conserved by lower affinity TCRs, suggesting a shared TCR–pMHC docking mode and an antigen-driven selection of the best-fitted TCR. In order to validate this hypothesis, we focused our attention on another high-avidity public TCR directed against the immunodominant HCMV epitope, RA15 (TRAV24–TRAJ49–TRBV6-1). Interestingly, RA15 has less avidity for NLV–A2 than RA14 (Trautmann *et al.*, 2005) and shares only three of the four motifs of RA14 that contact the NLV–A2 surface (Gras, Saulquin *et al.*, 2009).

As our attempts to produce soluble RA15 TCR heterodimers with the strategy used for RA14 was unsuccessful, we looked for methods to stabilize the α/β heterodimer. Indeed, several strategies have been developed to achieve this goal, some of which work for several TCRs: expression of single-chain variable domain (scFv; Gregoire *et al.*, 1996; Housset *et al.*, 1997), fusion with a coil-coiled heterodimeriza-

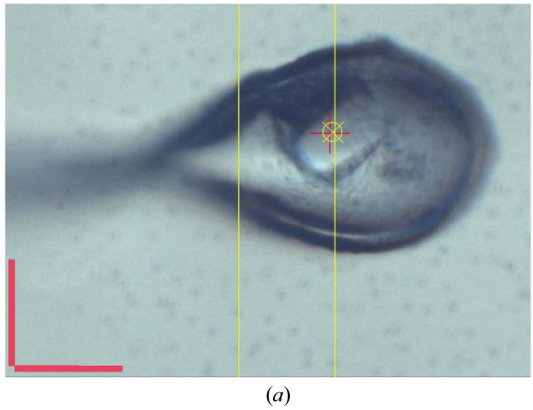

(*a*)

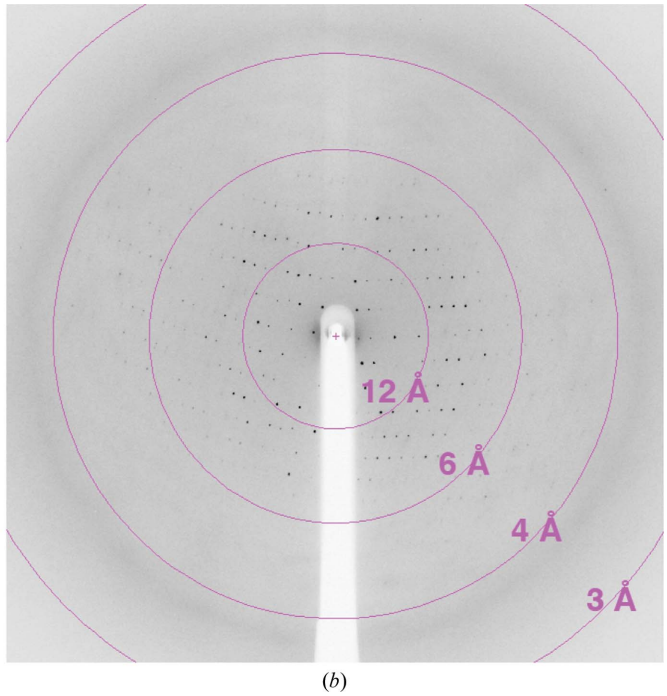

(*b*)

Figure 1
(*a*) View of the frozen RA15–NLV–A2 complex crystal in the loop. Scale bars represent 50 µm. (*b*) Diffraction pattern of the first 1° oscillation. Resolution circles and corresponding resolution are shown in pink.

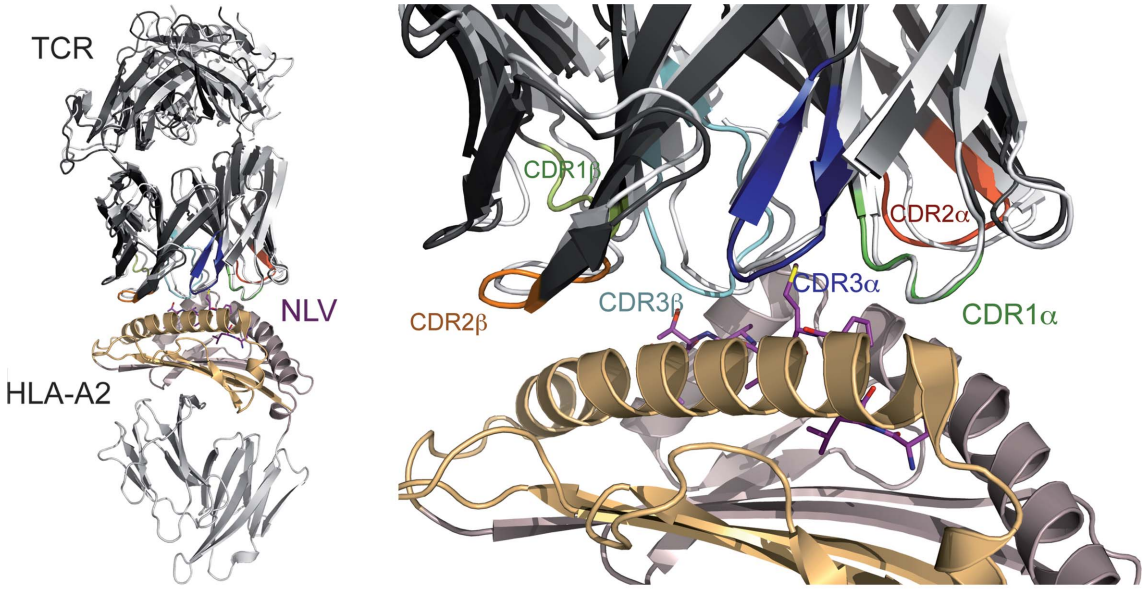

Figure 2
Superimposition of the molecular-replacement solution of the RA15–NLV–A2 complex (coloured) on the RA14–NLV–A2 complex structure (white). Superposition was performed on the $\alpha1\alpha2$ HLA-A2 domain. (*a*) Overall view of the superimposition, (*b*) closer view of the TCR–NLV–A2 interface. CDRs are coloured as follows: CDR1α, green; CDR2α, red; CDR3α, dark blue; CDR1β, pale green; CDR2β, orange; CDR3β, light blue. The NLV peptide is represented by violet sticks, the HLA-A2 $\alpha1$ helix in gold and the $\alpha2$ helix in silver.

tion motif (Willcox *et al.*, 1999), a membrane-proximal disulfide bridge (Stewart-Jones *et al.*, 2003) and a non-native interchain disulfide bridge (Boulter *et al.*, 2003). As the latter was successfully applied to characterize TCR–pMHC interactions (Boulter *et al.*, 2003) and ternary complex structure determination (Sami *et al.*, 2007; Archbold *et al.*, 2009; Dunn *et al.*, 2006; Tynan *et al.*, 2007; Gras, Burrows *et al.*, 2009), we decided to test it on RA15. By creating an artificial disulfide bridge between residue 48 of the Cα domain and residue 57 of the Cβ domain, we were able to produce several milligrams of cysteine mutated RA15 TCR in a soluble and homogeneous form and to crystallize it in complex with its cognate pMHC.

The crystallization strategy was based on the usage of commercial screening kits and home-made screens designed from the conditions in which other TCR–pMHC complexes were previously crystallized. This strategy appears to be suitable to find optimized conditions for a particular complex. Indeed, although TCR–pMHC ternary complexes are prone to crystallize in the presence of PEG, the buffer and pH, as well as the presence and type of secondary salts and additives, are critical to obtain well diffracting crystals. It is therefore necessary to test large screens of buffers and additives. To date, the best crystals of RA15–NLV–A2 appeared in the presence of 17–18% PEG 4000, 100 m*M* Tris pH 8.0–8.5 and $MgSO_4$ and the crystals tested diffracted to 4.7 Å resolution.

Using the single and complete data set obtained using synchrotron radiation, molecular replacement was employed to solve the low-resolution structure of the RA15–NLV–A2 complex as it crystallized in a different space group to that observed for RA14–NLV–A2 (Gras, Saulquin *et al.*, 2009). Rigid-body refinement was then performed at 4.7 Å resolution.

Although at a very low resolution, this new structure of a public TCR directed against the immunogenic NLV–HLA-A2 antigen provides some interesting structural features of the public nature of CMV epitope recognition. Indeed, the structure shows that RA15 docks on NLV-A2 in quite a similar way compared with the public RA14 TCR for which we have previously solved the structure. When the $\alpha1\alpha2$ A2 domains are superimposed, the RA15 variable domain has to be rotated by 8.5° with a pivotal point close to the tip of the Vα CDR1 loop and shifted by about 0.5 Å to be fitted onto the RA14 variable domain (Fig. 2). At the TCR–pMHC interface, the best superposed CDR is the CDR1 of the Vα domain with a 0.3 Å translational shift, while the positions of the five other CDRs vary from 1.1 to 2.7 Å for CDR2 of the Vβ domain. Quite logically, the most pronounced positional difference is observed for the domain that differs most in sequence. A small difference in the Vα–Vβ domain pairing of RA15 is also observed, with a rotation of 4.4° for the Vβ domain relative to the orientation of the Vβ domain in RA14. Despite these observed differences, the NLV–A2 surface buried by the RA15 TCR is likely to be very similar to that buried by RA14. However, owing to the resolution of the present structure of the RA15–NLV–A2 complex, it is not possible to obtain a detailed view of the interactions formed by this RA15 TCR to recognize its epitope. Higher resolution crystallographic data will be required. These may possibly be obtained by further crystallization screenings, either by using finer steps in screening around the already determined crystallization conditions or by looking for additives that may help to obtain crystals of better quality.

We thank the ID23-eh2 team for help with synchrotron data collection at ESRF (Grenoble, France), the staff of the EMBL HTX laboratory (Grenoble, France) for the use of the PSB crystallization platform and E. Forest (IBS, Grenoble, France) for the use of mass spectroscopy. This study was supported in part by the Agence Nationale de la Recherche (grant ANR-05-MIIM-019). MB was also supported by the EPI-PEPVAC European Union grant.

References

Archbold, J. K., Macdonald, W. A., Gras, S., Ely, L. K., Miles, J. J., Bell, M. J., Brennan, R. M., Beddoe, T., Wilce, M. C., Clements, C. S., Purcell, A. W.,

McCluskey, J., Burrows, S. R. & Rossjohn, J. (2009). *J. Exp. Med.* **206**, 209–219.
Bodinier, M., Peyrat, M. A., Tournay, C., Davodeau, F., Romagne, F., Bonneville, M. & Lang, F. (2000). *Nature Med.* **6**, 707–710.
Borysiewicz, L. K., Hickling, J. K., Graham, S., Sinclair, J., Cranage, M. P., Smith, G. L. & Sissons, J. G. (1988). *J. Exp. Med.* **168**, 919–931.
Boulter, J. M., Glick, M., Todorov, P. T., Baston, E., Sami, M., Rizkallah, P. & Jakobsen, B. K. (2003). *Protein Eng.* **16**, 707–711.
Diamond, D. J., York, J., Sun, J. Y., Wright, C. L. & Forman, S. J. (1997). *Blood*, **90**, 1751–1767.
Dunn, S. M., Rizkallah, P. J., Baston, E., Mahon, T., Cameron, B., Moysey, R., Gao, F., Sami, M., Boulter, J., Li, Y. & Jakobsen, B. K. (2006). *Protein Sci.* **15**, 710–721.
Engstrand, M., Tournay, C., Peyrat, M. A., Eriksson, B. M., Wadstrom, J., Wirgart, B. Z., Romagne, F., Bonneville, M., Totterman, T. H. & Korsgren, O. (2000). *Transplantation*, **69**, 2243–2250.
Garboczi, D. N., Hung, D. T. & Wiley, D. C. (1992). *Proc. Natl Acad. Sci. USA*, **89**, 3429–3433.
Gras, S., Burrows, S. R., Kjer-Nielsen, L., Clements, C. S., Liu, Y. C., Sullivan, L. C., Bell, M. J., Brooks, A. G., Purcell, A. W., McCluskey, J. & Rossjohn, J. (2009). *Immunity*, **30**, 193–203.
Gras, S., Saulquin, X., Reiser, J.-B., Debeaupuis, E., Echasserieau, K., Kissenpfennig, A., Legoux, F., Chouquet, A., Le Gorrec, M., Machillot, P., Neveu, B., Thielens, N., Malissen, B., Bonneville, M. & Housset, D. (2009). *J. Immunol.* **183**, 430–437.
Gregoire, C., Malissen, B. & Mazza, G. (1996). *Eur. J. Immunol.* **26**, 2410–2416.
Housset, D., Mazza, G., Gregoire, C., Piras, C., Malissen, B. & Fontecilla-Camps, J. C. (1997). *EMBO J.* **16**, 4205–4216.
Kabsch, W. (1993). *J. Appl. Cryst.* **26**, 795–800.
Lefranc, M. P. (2001). *Nucleic Acids Res.* **29**, 207–209.
McLaughlin-Taylor, E., Pande, H., Forman, S. J., Tanamachi, B., Li, C. R., Zaia, J. A., Greenberg, P. D. & Riddell, S. R. (1994). *J. Med. Virol.* **43**, 103–110.
Navaza, J. (1994). *Acta Cryst.* A**50**, 157–163.
Peggs, K., Verfuerth, S., Pizzey, A., Ainsworth, J., Moss, P. & Mackinnon, S. (2002). *Blood*, **99**, 213–223.
Quinnan, G. V. Jr, Burns, W. H., Kirmani, N., Rook, A. H., Manischewitz, J., Jackson, L., Santos, G. W. & Saral, R. (1984). *Rev. Infect. Dis.* **6**, 156–163.
Sami, M., Rizkallah, P. J., Dunn, S., Molloy, P., Moysey, R., Vuidepot, A., Baston, E., Todorov, P., Li, Y., Gao, F., Boulter, J. M. & Jakobsen, B. K. (2007). *Protein Eng. Des. Sel.* **20**, 397–403.
Saulquin, X., Ibisch, C., Peyrat, M. A., Scotet, E., Hourmant, M., Vie, H., Bonneville, M. & Houssaint, E. (2000). *Eur. J. Immunol.* **30**, 2531–2539.
Sissons, J. G., Bain, M. & Wills, M. R. (2002). *J. Infect.* **44**, 73–77.
Stewart-Jones, G. B., McMichael, A. J., Bell, J. I., Stuart, D. I. & Jones, E. Y. (2003). *Nature Immunol.* **4**, 657–663.
Trautmann, L., Rimbert, M., Echasserieau, K., Saulquin, X., Neveu, B., Dechanet, J., Cerundolo, V. & Bonneville, M. (2005). *J. Immunol.* **175**, 6123–6132.
Tynan, F. E., Reid, H. H., Kjer-Nielsen, L., Miles, J. J., Wilce, M. C., Kostenko, L., Borg, N. A., Williamson, N. A., Beddoe, T., Purcell, A. W., Burrows, S. R., McCluskey, J. & Rossjohn, J. (2007). *Nature Immunol.* **8**, 268–276.
Willcox, B. E., Gao, G. F., Wyer, J. R., O'Callaghan, C. A., Boulter, J. M., Jones, E. Y., van der Merwe, P. A., Bell, J. I. & Jakobsen, B. K. (1999). *Protein Sci.* **8**, 2418–2423.
Wills, M. R., Carmichael, A. J., Mynard, K., Jin, X., Weekes, M. P., Plachter, B. & Sissons, J. G. (1996). *J. Virol.* **70**, 7569–7579.